Numerical investigation of the reliability of wind-tunnel wall corrections applied to measurements of wingtip flow

Antoine Joulain, Damien Desvigne, David Alfano, Thomas Leweke

JOURNAL OF AIRCRAFT
Submitted – March 29, 2016

Numerical investigation of the reliability of wind-tunnel wall corrections applied to measurements of wingtip flow

Antoine Joulain*, Damien Desvigne†, David Alfano‡
AIRBUS HELICOPTERS SAS, 13725 Marignane, France

Thomas Leweke§
CNRS, Aix-Marseille Université, Centrale Marseille, 13384 Marseille, France

I. Introduction

HELICOPTER aerodynamics is strongly influenced by the vortices generated from the rotor blade tips. A literature survey highlights the lack of local blade tip flow measurements, mainly due to the complexity of the aerodynamic phenomena involved and the difficulty of measuring in a small region of interest. Fixed wings have been widely investigated experimentally and numerically to gain more insight into the tip vortex formation, the influence of the shape and the accuracy of the numerical codes (see, e.g. Brocklehurst and Barakos [1] and references therein). The database of McAlister and Takahashi [2] includes detailed measurements of the vortex roll-up in the vicinity of the wing tip, as well as vortex characteristics during the near-field propagation. It is one of the very few published experimental campaigns considering Reynolds numbers of more than one million, as well as the sensitivity to the tip shape, the Reynolds number and the angle of attack. Moreover, measurements are rectified for meandering, and corrections are proposed to account for wind-tunnel wall interference. In spite of its wealth, this database is used surprisingly rarely as a reference test case to validate numerical methods.

Lim [3] used the proposed wall corrections to simulate a free-air rounded-wing tip configuration without representing the overall experimental setup. The Thin-Layer compressible Navier-Stokes equations (TLNS) were solved with a second-order scheme and an algebraic turbulence model. The grid extended 8 chords downstream of the trailing edge and 6 chords around the profile, and was refined in the spanwise direction near the tip. The solution was in agreement with the measurements, but the leading-edge upper-surface suction peak and the tip vortex pressure footprint were not captured. Due to computational speed and memory constraints, no grid dependence study was undertaken. According to the author, the simulation could be improved in a number of ways: by increasing the mesh density in areas of high velocity gradients, performing a grid convergence study, extending the domain dimensions, using Reynolds-Averaged Navier-Stokes (RANS) instead of TLNS equations and by using a more physical turbulence model. The relevance of the wall corrections was not called into question.

Kamkar and Wissink [4] used McAlister and Takahashi's database [2] to perform a RANS simulation of the square-tip test case in free air, without wall corrections. An unstructured near-body grid was coupled with a structured off-body grid system. Adaptive Mesh Refinement, based on the Q-criterion [5], was performed on the off-body mesh and showed considerable improvements concerning the vortex convection. A difference of 15% for the velocity inside the vortex remained between the best calculation and the measurements, it was attributed to the dissipation of the unstructured near-body mesh and to the communication between unstructured and structured grids. The lack of wall corrections was not discussed, but represents probably a major contribution to the error.

The objective of the present work is to assess the accuracy of the wind-tunnel wall corrections published by McAlister and Takahashi [2]. To do this, a validated and efficient steady-state RANS method is used to simulate two- and three-dimensional configurations in free-air flow configurations. In this paper, the square-tip test case of McAlister and Takahashi [2] is investigated at an uncorrected chord-based Reynolds number $Re = 1.6 \times 10^6$, Mach number $M = 0.131$ and angle of attack $\alpha = 12°$.

*PhD Candidate, antoine.joulain@airbus.com
†Engineer, External Aerodynamics, damien.desvigne@airbus.com
‡Team Leader, External Aerodynamics, david.alfano@airbus.com
§Senior Researcher, IRPHE UMR 7342, thomas.leweke@irphe.univ-mrs.fr

II. Computational Setup

The configuration considered in the present simulations consists of a constant-chord NACA 0015 wing with a square tip, bounded at the root by a symmetry plane. The wing aspect ratio is small, it is therefore assumed rigid and free of aeroelastic deformations. Two coordinate systems are defined in the same way as for the experimental setup (presented in Section III). The first one is used to study forces and moments acting on the wing: the r- and ζ-axes extend respectively from the experimental root to the tip and from the leading edge to the trailing edge, the origin being at the root leading edge of the experimental geometry. The Eiffel frame (x, y, z) is employed to follow the tip vortex: the x-axis is aligned with the (horizontal) inflow direction; the y-axis extends from the tip to the root of the wing and the z-axis is vertical; moreover the origin is located at the center of the vortex core.

II.A. Numerical Method

The ONERA CFD code *elsA* [6] is used in this study. The solver is based on a cell-centered, finite-volume approach. Assuming a steady flow field, the compressible RANS equations are solved in two-dimensional (2D) and three-dimensional (3D) configurations on a multi-block structured grid. A fully turbulent flow is considered, without boundary-layer transition.

The governing equation system is closed with the one-equation model of Spalart and Allmaras [7]. Based on the Boussinesq assumption, this formulation was initially designed for the simulation of wall-bounded flows. In order to reduce the production of eddy viscosity in areas where the vorticity is higher than the strain rate (e.g. inside vortex cores), the rotation and streamline curvature correction proposed by Spalart and Shur [7] is applied.

The convective fluxes of the mean flow equations are discretized using the second-order central scheme of Jameson, Schmidt and Turkel [8]. Since this scheme is non-dissipative and unstable, a matrix artificial dissipation is introduced. The fourth-order coefficient $\kappa^{(4)}$ dampens the high-frequency oscillations in the bulk of the computational domain and is important for stability and convergence to a steady state. Typical values for $\kappa^{(4)}$ are in the range 0.016 to 0.032 [9]. In order to reduce the amount of dissipation being introduced and to improve the accuracy, $\kappa^{(4)}$ is taken as 0.016. The convective fluxes of the turbulence equations are discretized using a second-order Roe scheme [10]. All diffusive flux gradients are calculated with a five-point central scheme. A first-order backward-Euler scheme updates the steady-state solution and the LU-SSOR (Lower-Upper Symmetric Successive Over-Relaxation) scheme [11] is employed to speed up convergence.

The resulting flow solver is implicit and stable, and high values of the Courant-Friedrichs-Lewy (CFL) number can be reached. The CFL number is linearly ramped up from 1 to 10 over 100 iterations, in order to avoid divergence during the transient phase. The L^2 norm-based residual of the total energy per unit volume, $\mathfrak{R}$, is used to measure the convergence of the simulations.

II.B. Computational Grid

The structured grids are generated using the ANSYS ICEM-CFD software, and all lengths are normalized by the wing chord c. The initial mesh is designed for industrial use and is universally applicable, without prior knowledge of the final solution. In particular, the vortex trajectory is not used to align the main grid axis and to refine the mesh in the zone covering the vortex core. This choice allows a wide variation of angle of attack, free-stream velocity and geometry.

The mesh results from an exhaustive grid-independence study concerning each construction parameter (documented in Ref. [12]). A C-topology surrounds the 2D NACA 0015 profile and an H-topology covers the downstream zone. In the spanwise direction, an H-topology is also chosen to match the square wing tip. The computational domain extends up to a distance of $200c$ in all directions from the tip in order to minimize the influence of boundary conditions. Thus the numerical wing has a span of $200c$. The difference between experimental and numerical wing spans is not detrimental to the study of the vortex roll-up in the vicinity of the tip, as the root circulation is transferred into the trailing sheet.

The 2D mesh around the NACA 0015 profile is constructed as follows. In the streamwise direction, the leading-edge grid spacing is equal to $10^{-4}c$ and the trailing-edge grid spacing is $2 \times 10^{-4}c$. The blunt trailing edge (of thickness $3.15 \times 10^{-3}c$) is finely discretized with a grid spacing of $8.3 \times 10^{-6}c$ at the corners. The mesh distribution around the profile follows geometric progressions starting from each specified grid spacing. The common ratio of a geometric progression is called expansion ratio. The expansion ratio on the profile is lower than 1.06. In the wall-normal direction, the first grid spacing is set to $8.3 \times 10^{-6}c$ for a dimensionless wall distance (y^+, see e.g. Ref. [13]) around unity at the first computational nodes. At 12° incidence and Reynolds number 1.5×10^6, the computed y^+ is maximal at the suction peak with a value of 1.5, and it does not exceed 0.5 on the lower side of the profile. The wall-normal expansion ratio is set to 1.15 and is not relaxed away from the profile in order to preserve the orthogonality of the cells. Downstream of the trailing edge, the first grid spacing is equal to the trailing-edge grid spacing and an expansion ratio of 1.1 is applied. The distribution on the outer boundary is manually adapted to maximize the orthogonality of the mesh at the wall. The resulting 2D mesh contains 7×10^5 points.

The 3D mesh is constructed by stacking 2D meshes along the r-axis. The boundary layer developing around the square tip is simulated with a spanwise tip spacing of $5 \times 10^{-5}c$. The maximum value of the dimensionless wall distance y^+ reaches 8 and is located in the vicinity of the leading edge. A spanwise expansion ratio of 1.01 is imposed throughout the fluid domain, as well as from the tip to the root of the wing. In the fluid domain, the gap resulting from the 2D mesh stacking is filled with a half-butterfly mesh (O-grid mesh), which inevitably induces two lines of skewed cells near the fictitious leading edge. The wall-normal grid spacing and expansion ratio are used in the gap domain. The final mesh contains 4.4×10^7 points and is split into 137 blocks to enable parallel processing. The values of the grid parameters are summarized in Table 1.

Table 1. Grid parameters

Domain dimension	$(400c)^3$
Leading-edge streamwise spacing	$10^{-4}c$
Trailing-edge streamwise spacing	$2 \times 10^{-4}c$
Profile streamwise expansion ratio	1.06
Wall-normal first spacing	$8.3 \times 10^{-6}c$
Wall-normal expansion ratio	1.05
Downstream first spacing	$2 \times 10^{-4}c$
Downstream expansion ratio	1.1
Spanwise tip spacing	$5 \times 10^{-5}c$
Spanwise expansion ratio	1.01

The wing surface is modeled as an adiabatic viscous wall (zero heat-flux). The outer boundary supporting the root of the wing is a symmetry plane, whereas a far-field condition is applied to all other external boundaries.

III. Experimental Database

McAlister and Takahashi's [2] wing consisted of a constant and untwisted NACA 0015 profile with a square tip. The chord (c) and semi-span (R) were respectively 0.52 m (1.7 ft) and 1.7 m (5.6 ft). The width (w) and the height (h) of the test section were 3 m (10 ft) and 2.1 m (7 ft). The wing was mounted on a 6.4 cm (2.5 in) thick supporting end plate extending from floor to ceiling. In the lateral direction, the tip of the wing and the supporting end plate were positioned respectively at 1 m (3.3 ft) and 0.3 m (1 ft) from the wind tunnel walls. A cylindrical tube fairing was placed between the supporting end plate and the wall. In order to perform 2D measurements, a second end plate was positioned against the tip, preventing the development of a trailing vortex. The transition of the boundary layers was not forced.

Wing surface pressure (coefficient C_p) was measured at 320 stations, with a denser distribution near the leading edge and the tip. The measurement section nearest the tip was located at a distance of 2% of the chord c, i.e. at $r/R = 0.994$. Lift (C_l), pressure-drag and pitching moment coefficients were calculated from a trapezoidal-rule integration of the pressure distribution. The pitching moment coefficient is defined about the quarter-chord and is taken as positive when the angle of attack is increasing. Results are published in the Eiffel frame (with respect to the undisturbed flow). A two-components laser velocimeter is used to measure the vertical (V_z) and the axial (V_x) velocity profiles across the trailing vortex along the y-axis. Measurements are made at streamwise locations from $0.1c$ to $6c$ behind the wing.

III.A. Blockage Correction

During the experiment, the reference velocity is obtained from a Pitot-static probe placed upstream in the test section. The experimental assembly generates a blockage resulting in a higher velocity in the region where the airfoil is located. The uncorrected reference velocity $V_{\infty,u}$ (and consequently the Mach number, Reynolds number and all aerodynamic coefficients) has to be corrected according to

$$V_\infty = (1 + \varepsilon) V_{\infty,u} \tag{1}$$

The value of the blockage factor ε, in 2D and 3D configurations, is estimated using a simple formula based on the area reduction induced by each object in the tunnel [14]:

$$\varepsilon = b \frac{\text{Object frontal area}}{\text{Test section area}} \tag{2}$$

with $b = 0.25$ for the airfoil and $b = 1$ otherwise. The additional blockage resulting from the development of the tunnel boundary layers and the wing wake is not taken into account. According to the published geometry of the assembly, the total blockage factor, at an angle of attack $\alpha = 12°$, is $\varepsilon = 0.06$ in the 2D configuration and $\varepsilon = 0.04$ in the 3D configuration. The blockage factor of the airfoil is weakly dependent on the angle of attack and represents 13% and 20% of the total blockage in 2D and 3D, respectively. End plates are the major contributors, with 70% of the total blockage in the 2D configuration (two end plates) and 54% in the 3D configuration. For the former, this leads to a reduction of the force and moment coefficients by about 12%.

Velocity profiles reveal that far from the wing tip vortex (and the wing trailing sheet), the streamwise velocity tends neither to the uncorrected nor to the corrected reference velocity, but converges to a value between 1.1 $V_{\infty,u}$ (at $x_t/c = 0.1$) and 1.07 $V_{\infty,u}$ (at $x_t/c = 4$). The boundary layers developing on the supporting plate and the tunnel walls, as well as the wake, may induce an additional blockage and an increase of the local velocity downstream of the profile. However, the observed deviation of the axial velocity from the corrected reference value is rather erratic and does not increase with downstream distance. A calibration error of the laser velocimeter could be responsible for such discrepancies. Two methods can be used to correct the vertical and axial velocities: the first is to increase the blockage factor (up to 0.1 at $x_t/c = 0.1$), and the second to apply the blockage factor calculated from Equation (2) and shift the corrected measurements to recover V_∞ far from the vortex. The two methods give similar results, and the first one is retained.

III.B. Lift Interference Correction

The walls of the closed test section confine the airflow and distort the streamlines around the lifting body.

In the 2D configuration, Lock's [15] method for taking this effect into account consists in replacing the lifting airfoil by a single vortex at the center of pressure. The floor and ceiling of the tunnel are mathematically represented by an infinite series of image vortices, in order to satisfy the absence of normal flow at the walls. The angle of attack α and the lift coefficient C_l of the profile are modified by the velocity induced by these image vortices. Assuming a profile centered in the test section, a short chord c relative to the tunnel height h and a small angle of attack, the corresponding corrections were given by Allen [16] as:

$$\begin{aligned} \alpha &= \alpha_u + \frac{180}{\pi}\frac{\pi c^2}{96\beta h^2}(C_{l,u} + 4C_{m,u}) \quad \text{and} \\ C_l &= \left[1 - \frac{1}{3}\left(\frac{\pi c}{4\beta h}\right)^2\right] C_{l,u} \quad \text{with} \\ \beta &= \sqrt{1 - M_u^2} \end{aligned} \tag{3}$$

The low Mach numbers considered here allow to assume an incompressible flow (compressibility factor $\beta = 1$). Due to the small value of the ratio c/h (0.25), the lift interference correction in the 2D configuration is very small: the angle of attack is increased by 1% and the lift coefficient is decreased by 1.6%.

In the 3D configuration, the half-model is treated as a complete wing in a tunnel with twice the cross section, with the side-wall as a symmetry plane. The lifting wing is replaced by a semi-infinite vortex pair trailing from the tips. The walls of the tunnel are now represented by a doubly-infinite series of vortex images. Assuming again a small wing compared to the dimensions of the tunnel, only the angle of attack is modified according to [17]

$$\alpha = \alpha_u + \delta_E \frac{180}{\pi}\left(1 + \frac{c\delta_1}{2\beta h \delta_0}\right)\frac{A}{A_t} C_{l,u} \tag{4}$$

where A is the planform area of the semi-span wing (Rc), A_t the cross-sectional area of the tunnel (wh), and where δ_E, δ_0 and δ_1 depend only on the geometric parameters $2w/h$ and R/w. Detailed expressions and charts can be found in Ref. [17] and Ref. [18]. For the present experiment, with $2w/h = 2.86$ and $2R/b = 0.56$, these parameters are estimated as $\delta_E = 0.05$, $\delta_0 = 0.19$ and $\delta_1 = 0.42$, respectively. Assuming an incompressible flow ($\beta = 1$), the correction in Equation (4) is directly proportional to the lift coefficient and increases the incidence by 4.3% at 12°.

The trajectory of the tip vortex is also influenced by the walls of the tunnel. In free air, the vortex pair generated by a lifting wing is deflected downward by mutual induction. In the tunnel, the walls, or the equivalent doubly-infinite series of images, generate induced velocities acting on the tip vortex. The wing and trailing vortex are centered in the vertical direction in the tunnel, thus the interference concerning the horizontal displacement of the tip vortex is very small. On the contrary, in the lateral direction the tip of the wing and the trailing vortex are closer to the opposite side wall than to the supporting end plate. Thus the lift interference on the vertical displacement is quite substantial. Due to this up-wash the tip vortex is actually measured to move upward, which is not consistent with the behavior in free air.

IV. Comparison Between Simulation and Experiment

IV.A. Two-Dimensional Flow

The 2D test case of McAlister and Takahashi [2] at $Re = 1.5 \times 10^6$ ($M = 0.124$) is calculated for angles of attack in the range $0° \le \alpha \le 14°$, in steps of 1°. The blockage correction increases the Reynolds number to 1.6×10^6 ($M = 0.131$). The lift interference correction is taken into account in the CFD simulations.

In order to study the convergence history, 100,000 iterations are performed at a (corrected) incidence of $\alpha = 12.13°$. The residual $\mathfrak{R}$ drops by six orders of magnitude. After 12,000 iterations, the variation of lift and pressure drag is less than 1% of the converged values.

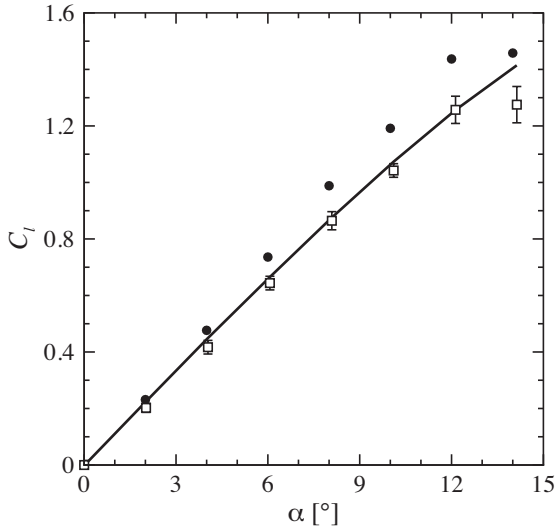

Figure 1. Lift coefficient as function of angle of attack for the 2D configuration at $Re = 1.6 \times 10^6$ and $M = 0.131$. numerical solution (—), uncorrected (•) and corrected (□) experimental data from McAlister and Takahashi [2].

20,000 iterations are required to reach an error below 0.1%. Approximately three hours are needed to achieve 20,000 iterations on six cores of Intel Xeon E5-2697 v2 processors at 2.7 GHz interconnected with an Infiniband FDR network and with 48 Go of RAM.

The dependence of the lift coefficient on angle of attack is plotted in Fig. 1. Its variation along the span of the wing in the experiments appears as error bars on the symbols. In the case of a purely 2D flow, no spanwise variation is expected. The observed deviation depends weakly on the angle of attack in the range $0 \le \alpha \le 10°$ and can be interpreted as the experimental measurement scatter. For $\alpha > 10°$, this variation increases, indicating the additional influence of a 3D stall phenomenon.

Figure 1 reveals a significant difference between the uncorrected lift measurements and the simulation results. At $\alpha = 12°$, this difference reaches 16%. The blockage correction greatly improves the agreement, the deviation at $\alpha = 12°$ being reduced to 3%, and even to 1% when applying the lift interference correction. The agreement is poor at $\alpha = 14°$. Experimentally, the 2D assumption at this incidence is less justified, because the variation along the span is high and the flow is probably stalled. According to the review of 2D experimental databases published by McCroskey [19], the measurement of maximum lift at low Mach number suffers from a high dispersion, partly due to wind tunnel wall effects. Concerning simulation aspects, the RANS equations have previously shown low efficiency with the simulation of 2D stalled flow [20,21]. One of the main causes is the inadequacy of the boundary-layer transition model to simulate leading-edge laminar-bubble separation and expansion up to stall.

IV.B. Three-Dimensional Flow

The accuracy of the 3D corrections is now investigated by a comparison between the numerical simulation and the 3D experimental database of McAlister and Takahashi [2]. The square-wing tip test case is used at Reynolds number $Re = 1.6 \times 10^6$, Mach number $M = 0.131$ and angle of attack $\alpha = 12°$. The blockage correction (III.A) increases the Reynolds number to $Re = 1.7 \times 10^6$ and the Mach number to $M = 0.140$. The lift interference correction (III.B) increases the angle of attack to $\alpha = 12.5°$.

In order to assess the convergence of the 3D solution, a simulation with 100,000 iterations was performed, requiring approximately 50 hours of calculation on 150 cores. During the first 40,000 iterations, the residual $\mathfrak{R}$ drops by four orders of magnitude. It then stagnates until the end of the calculation. The same trend is observed for all other conservative variables, including turbulent ones. The main cause for this stagnation is localized at the leading edge of the tip section. In

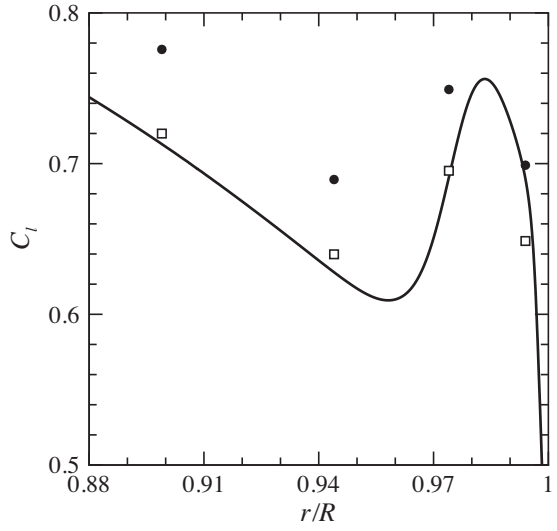

Figure 2. Sectional lift coefficient along the span in the vicinity of the tip. Numerical simulations (—), uncorrected (•) and corrected (□) experimental data from McAlister and Takahashi [2].

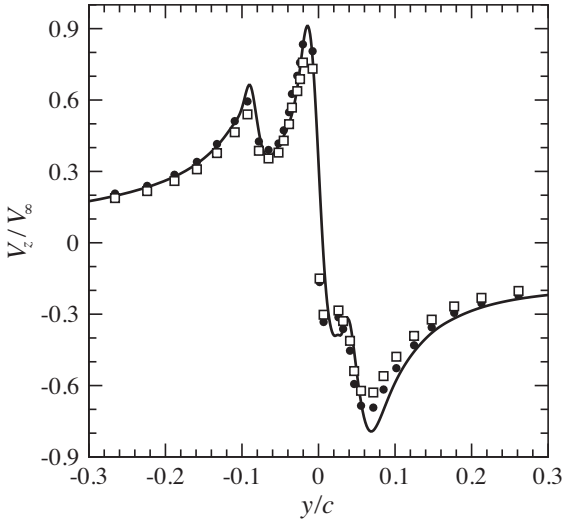

Figure 4. Vertical velocity profiles across the vortex core at 0.1 chord downstream of the trailing edge. Numerical simulation (—), uncorrected (•) and corrected (□) experimental data from McAlister and Takahashi [2].

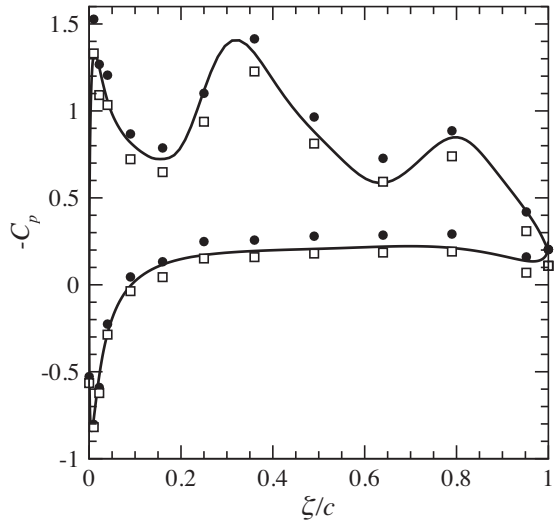

Figure 3. Pressure coefficient along the chord at r/R = 0.994. Numerical simulation (—), uncorrected (•) and corrected (□) experimental data from McAlister and Takahashi [2].

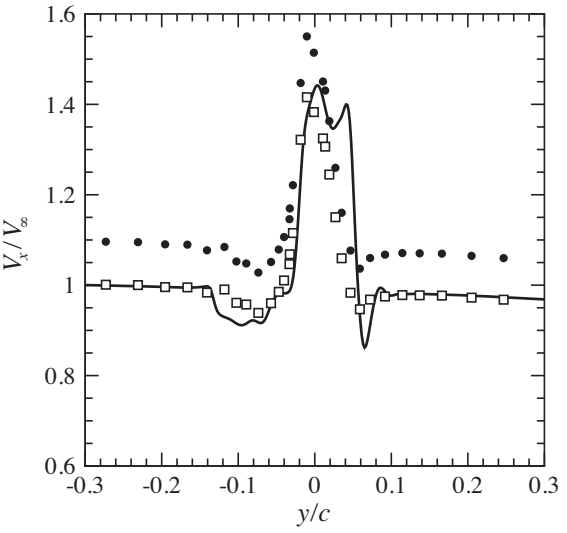

Figure 5. Axial core velocity profiles across the vortex at 0.2 chord downstream of the trailing edge. Numerical simulation (—), uncorrected (•) and corrected (□) experimental data from McAlister and Takahashi [2].

this area, the geometric truncation produces sharp edges, responsible for flow separation and a destabilization of the solution. The residual, which is an integrated value over the whole domain, is polluted by this local fluctuation. Nevertheless, the low CFL number employed prevents the propagation of this instability beyond a few tenth of a percent of the chord from the tip leading edge.

The vortex generation process alters the pressure in the vicinity of the wing tip. The low-pressure footprint generated on the upper surface is responsible for additional lift, pressure drag and pitching moment peaks. In the vortex footprint, the three sectional coefficients converge very well, but at different speeds. After 20,000 iterations, the resulting C_l reaches the converged value (obtained with the 100,000-iteration calculation) to within 0.25%. The convergence of the drag and pitching moment coefficients is slower, and the results are within 0.4% and 0.6% of the converged values, respectively. Far away from the tip, in the inner part of the wing, the convergence of the aerodynamic coefficients is identical to the purely 2D configuration presented in Section IV.A.

From the blade root to the blade tip, and in particular from r/R = 0.88 to the tip (Fig. 2), the corrected experimental lift coefficient is in good agreement with the calculated one. Similar agreement is obtained for the pressure drag and the pitching moment coefficients.

At $r/R = 0.370$ and $r/R = 0.974$, the numerical pressure coefficient profiles and the corrected measurements are in good agreement, which demonstrate the validity of the wall corrections. At $r/R = 0.994$ (Fig. 3), the three upper-side suction peaks are found at the same position along the chord. The two pressure peaks at the leading-edge (upper side and lower side) are in good agreement. However, the simulation overestimates the amplitude of the first (at $\zeta/c \approx 0.3$) and second (at $\zeta/c \approx 0.8$) vortex footprints by 9% and 14%, respectively. The numerical results are always located between the uncorrected and the corrected measurements. The deviation on the lower side of the wing is surprising, it could be due to the application of an excessive blockage correction to the measurements. Considering the rough approximation of Eq. (2), the deviation remains acceptable.

Numerically, the "main vortex" center is identified, from the trailing edge up to 6 chords behind the wing by the maximum value of the Q-function [5]. From the trailing edge up to $0.5c$ downstream, the simulated and measured main vortex trajectories are in good agreement.

Beyond 1 chord downstream of the trailing edge, the horizontal displacements slightly diverge and result in a 10% deviation at 6 chords. In the vicinity of the wing, the measured vertical displacement is not influenced by the wind tunnel walls and matches the simulation result. From 1 chord downstream, the experimental values are clearly influenced by the tunnel walls and are not comparable to a free-air simulation.

Velocity profiles are extracted on a horizontal line passing through the main vortex center, in order to mimic the experimental procedure. The measured profiles are corrected with a suitable blockage factor (see Section III.A), in order to recover $V_x/V_\infty = 1$ far from the vortex and the wing trailing sheet.

At 0.1 chord downstream of the trailing edge (Fig. 4), the vertical velocity amplitude is lower than unity and the application of the correction has little influence. The two maxima observed on the vertical velocity profile (at $y/c \approx$ -0.09 and -0.02) are well located. The simulation overestimates the first maximum by 20%, compared to the corrected measurement. A precise comparison cannot be made concerning the maximum and minimum vertical velocities; nevertheless, the experimental values and the numerical result are consistent. In particular, the small double inflection seen at $y/c \approx 0.02$ is present in both cases. At $y/c \approx 0.07$, the simulation exhibits a local deviation of 25% with respect to the corrected measurement.

At 0.2 chord downstream of the trailing edge (Fig. 5), the corrected measurements and the calculated axial velocity profile are in good agreement. The maximum amplitudes are identical, the large low-velocity region between $y/c \approx$ -0.12 and -0.04 is similar, and the small low-velocity region at $y/c \approx 0.06$ is visible. Contrary to the measurements, the numerical solution exhibits a second peak at $y/c \approx 0.04$.

V. Conclusions

To conclude, concerning the 2D test case at Reynolds number 1.6×10^6 and Mach number 0.131, good agreement is found between the numerical solution and the corrected measurements. On the one hand, the numerical method is fast and gives accurate solutions, as long as the airfoil does not approach stall. On the other hand, the blockage correction and the lift interference correction given by Equations (2) and (3) are well suited and reveal the high quality of the database. Except near stall angles, where the 2D assumption becomes invalid, the corrected mean values of pressure, lift and pitching moment coefficients match the numerical results.

Concerning the 3D square-wing tip test case at Reynolds number $Re = 1.6 \times 10^6$, Mach number $M = 0.131$ and angle of attack $\alpha = 12°$, the corrected experimental measurements and the numerical solution are in good agreement regarding the mean aerodynamic coefficients on the wing and the mean vortex characteristics in the near field (up to 1 chord downstream of the trailing edge). The basic wall corrections proposed by McAlister and Takahashi [2] are found to be necessary and reliable. They produce results consistent with free-air simulations, even if the employed blockage factor appears slightly too high for the measurements close to the tip. Between the trailing edge and 0.5 chord behind the wing, the simulated vortex trajectory agrees well with the measurements, even in the vertical direction, where the influence of the tunnel walls is known to be strong. In order to recover the reference velocity far from the vortex and the wing trailing sheet, the vertical and axial velocity measurements are corrected with an *ad hoc* method. A good match is found between corrected experiment and simulation for the vortex roll-up, concerning the amplitude and location of the velocity peaks, as well as the medium- and high-frequency variations of the velocity profiles.

Deviations between numerical solution and measurements are probably related to the use of steady-state simulations. Nevertheless, this efficient numerical method allows a detailed physical analysis of the vortex roll-up around the square wing tip in order to understand the origin and development of the multiple variations observed in the pressure and velocity profiles. The same numerical method is used in Ref. [12] to compute different test cases of McAlister and Takahashi's database [2], including variations of tip shape, Reynolds number and angle of attack variations.

References

[1] Brocklehurst, A. and Barakos, G. N., "A Review of Helicopter Rotor Blade Tip Shapes," *Progress in Aerospace Sciences*, Vol. 56, 2012, pp. 35–74, doi:10.1016/j.paerosci.2012.06.003.

[2] McAlister, K. W. and Takahashi, R. K., "NACA 0015 Wing Pressure and Trailing Vortex Measurements," NASA TP-3151, 1991.

[3] Lim, H.-B., "Numerical Study of the Trailing Vortex of a Wing With Wing-Tip Blowing," NASA CR-195803, 1994.

[4] Kamkar, S. J., Jameson, A., Wissink, A. M., and Sankaran, V., "Automated Off-Body Cartesian Mesh Adaptation for Rotorcraft Simulations," AIAA Paper 2011-1269, *49th Aerospace Sciences Meeting Including the New Horizons Forum and Aerospace Exposition*, Jan. 2011, pp. 17298–17322, doi:10.2514/6.2011-1269.

[5] Jeong, J. and Hussain, F., "On the Identification of a Vortex," *Journal of Fluid Mechanics*, Vol. 285, 1995, pp. 69–94, doi:10.1017/S0022112095000462.

[6] Cambier, L., Heib, S., and Plot, S., "The Onera elsA CFD Software: Input From Research and Feedback From Industry," *Mechanics & Industry*, Vol. 14, No. 3, 2013, pp. 159–174, doi:10.1051/meca/2013056.

[7] Spalart, P. R. and Allmaras, S. R., "A One-Equation Turbulence Model for Aerodynamic Flows," AIAA Paper 1992-0439, *30th Aerospace Sciences Meeting & Exhibit*, Jan. 1992, doi:10.2514/6.1992-439.

[8] Jameson, A., Schmidt, W., and Turkel, E., "Numerical Solution of the Euler Equations by Finite Volume Methods Using Runge-Kutta Time-Stepping Schemes," AIAA Paper 1981-1259, *14th Fluid and Plasma Dynamics Conference*, June 1981, doi:10.2514/6.1981-1259.

[9] Swanson, R. C., Radespiel, R., and Turkel, E., "On Some Numerical Dissipation Schemes," *Journal of Computational Physics*, Vol. 147, No. 2, 1998, pp. 518–544, doi:10.1006/jcph.1998.6100.

[10] Roe, P. L., "Approximate Riemann Solvers, Parameter Vectors, and Difference Schemes," *Journal of Computational Physics*, Vol. 43, No. 2, 1981, pp. 357–372, doi:10.1016/0021-9991(81)90128-5.

[11] Yoon, S. and Jameson, A., "An LU-SSOR Scheme for the Euler and Navier-Stokes Equations," AIAA Paper 1987-0600, *25th Aerospace Sciences Meeting*, Jan. 1987, doi:10.2514/6.1987-600.

[12] Joulain, A., "Aerodynamic Simulations of Helicopter Main-Rotor Blade Tips," PhD Thesis, University of Aix-Marseille, 2015.

[13] Tennekes, H. and Lumley, J. L., *A First Course in Turbulence*, MIT Press, 1972, ISBN: 9780262200196.

[14] Rae, W. H. and Pope, A., *Low-Speed Wind Tunnel Testing*, John Wiley & Sons, Inc., 2nd ed., 1984, ISBN: 9780471874027.

[15] Lock, C. N. H., "The Interference of a Wind Tunnel on a Symmetrical Body," British A.R.C. R&M-1275, 1929.

[16] Allen, H. J. and Vincenti, W. G., "Wall Interference in a Two-Dimensional-Flow Wind Tunnel, with Consideration of the Effect of Compressibility," NACA TR-782, 1944.

[17] Garner, H. C., Rogers, E. W. E., Acum, W. E. A., and Maskell, E. C., "Subsonic Wind Tunnel Wall Corrections," AGARDograph 109, 1966.

[18] Glauert, H., "Wind Tunnel Interference on Wings, Bodies and Airscrews," British A.R.C. R&M-1566, 1933.

[19] McCroskey, W. J., "A Critical Assessment of Wind Tunnel Results for the NACA 0012 Airfoil," NASA TM-100019, 1987.

[20] Szydlowski, J. and Costes, M., "Simulation of Flow Around a NACA0015 Airfoil for Static and Dynamic Stall Configurations Using RANS and DES," *American Helicopter Society 4th Decennial Specialists' Conference on Aeromechanics*, Jan. 2004.

[21] Moulton, M. A., Wong, T.-C., Smith, M. J., Le Pape, A., and Le Balleur, J.-C., "The Role of Transition Modeling in CFD Predictions of Static and Dynamic Stall," *37th European Rotorcraft Forum*, Sept. 2011, pp. 1097–1108, ISBN: 9781618396266.